Temperature-Dependent Antiferromagnetic Exchange Along 1D Linear Regular Chains of Phthalonitrile Blatter Radical

Nicolas Chrysochos,[a] Christos P. Constantinides,*[,b] Gregory Leitus,[c] Andreas Kourtellaris,[a] Daniel B. Lawson,[b] Mercè Deumal,[d] Jordi Ribas-Ariño,[d] Maria Àngels Carvajal,[d] Georgia A. Zissimou,[a] Constantinos Nicolaides,[e] Theodossis Trypiniotis,[e] and Panayiotis A. Koutentis[a]

[a] Department of Chemistry, University of Cyprus, P.O. Box 20537, 1678 Nicosia, Cyprus

[b] Department of Natural Sciences, University of Michigan – Dearborn, 4901 Evergreen Rd, Dearborn, MI 48128, United States

[c] Department of Organic Chemistry, Weizmann Institute of Science, 76100 Rehovot, Israel

[d] Departament de Ciència de Materials i Química Física & Institut de Química Teòrica i Computacional (IQTCUB), Universitat de Barcelona, Martí i Franquès 1, E-08820, Barcelona

[e] Department of Physics, University of Cyprus, P.O. Box 20537, 1678 Nicosia, Cyprus

Abstract

1,3-Diphenyl-1,4-dihydrobenzo[*e*][1,2,4]triazin-4-yl-6,7-dicarbonitrile is an exceptionally stable electron deficient organic radical with a promising potential to be used as a building block in a range of electronic and spintronic materials. The radical has a fully reversible one electron redox and is highly delocalized with some spin density reaching as far as the nitrile groups. Two polymorphs, ***α*** and ***β***, have been identified and characterized by single crystal X-ray diffractometry. Both polymorphs form one dimensional (1D) π-stacks. However, while in polymorph ***α*** radicals are located at evenly interplanar distances (3.366 Å), in polymorph ***β*** radicals are located at alternate interplanar distances (3.182 and 3.318 Å). Magnetic susceptibility measurements for polymorph ***α*** indicate strong antiferromagnetic interactions along the 1D regular chain. Magnetic susceptibility data cannot be fully fitted to the Bonner and Fischer model for the 2–300 K temperature range. The

steeper rise in paramagnetism above 80 K was rationalized by temperature-dependent antiferromagnetic exchange interactions between radicals within the 1D π stacks, which is indeed supported by DFT calculations. A microscopic study of the magnetic topology of polymorph $\boldsymbol{\alpha}$ together with the interpretation of its magnetic experimental data was pursued using a *First-Principles Bottom-Up* approach. Minuscule changes in crystal packing upon changing temperature significantly affect the magnetic interaction between spin-containing moieties. Temperature, therefore, is the key player in rationalizing the magnetism in polymorph $\boldsymbol{\alpha}$.

Introduction

Gombergs' discovery of the first organic radical in 1900 led to the development of numerous *persistent* and *stable* organic radicals with applications in the biological and material sciences.[1] While *persistent* radicals have sufficient lifetimes under inert conditions to be observed by spectroscopic methods, *e.g.*, EPR, UVv-Vis etc., *stable* radicals possess oxygen, moisture and thermal stability and therefore can be isolated, stored and studied under ambient conditions.[2]

Hydrazyls contain a divalent nitrogen $R_2N-N^{\bullet}-R$ and are usually persistent radicals.[2] Some analogues, *e.g.*, *N,N′*-diphenyl-*N′*-picrylhydrazyl (DPPH), have exceptional stability.[3] Several radical families, *e.g.*, verdazyls and 1,2,4-benzotriazinyls, incorporate the hydrazyl moiety into their skeletons.[2,4] Constraining the hydrazyl group inside a ring optimizes the delocalization of the unpaired spin (resonance stabilization) and provides electronic protection to the radical.[2,5] This is particularly true for 1,2,4-benzotriazinyls (Blatter radicals) where the unpaired spin is not only delocalized over the three nitrogen atoms of the triazinyl moiety but also over the benzo-fused portion.[4,6-8] These radicals have exceptional stability towards oxygen and moisture.[4] They also possess thermal stability that allows for sublimation without degradation. This intrinsic property has been used in thin film preparation.[9,10]

H. M. Blatter first prepared 1,3-diphenyl-1,4-dihydrobenzo[*e*][1,2,4]triazin-4-yl (**1**) (Figure 1) in 1968.[11] With the exception of a few EPR/X-ray studies,[12-16] this radical system did not receive much attention until 1996 when Wudl showed it formed a pressure sensitive semiconductor with tetracyanoquinodimethane (TCNQ).[17]

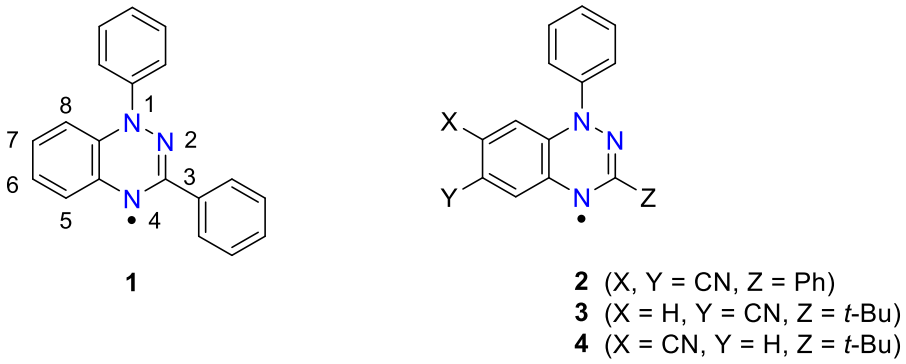

1

2 (X, Y = CN, Z = Ph)
3 (X = H, Y = CN, Z = *t*-Bu)
4 (X = CN, Y = H, Z = *t*-Bu)

Figure 1. Molecular structures of 1,2,4-benzotriazinyls **1** (Blatter radical) and **2-4** showing atom numbering.

Owing to their exceptional stability, we have systematically developed new synthetic procedures that broadened access to various derivatives,[18-24] and significantly expanded the structural diversity of the parent radical **1**. Consequently, the interest in this family of radicals has been reignited.[25-27] Many new physical properties and applications have now been reported.[4,10,28-41] The magnetic properties of these radicals are dominated by their propensity to form one-dimensional (1D) π stacks maximizing the SOMO-SOMO overlap of the radicals along the stacking direction. 1D ferro- and anti-ferromagnetism have been reported[28,31,35,37-41] along with two examples of magnetic-bistability associated with a first order structural phase transition.[32,36] Blatter radicals have been used in chemical synthesis as initiators in controlled polymerizations,[42-45] as ligands in coordination complexes with paramagnetic metals[46-48] and metal-organic frameworks (MOFs),[49] and as building units in diradicals and biradicaloids.[9,39,50] Their optical properties stem from their low-lying SOMO orbital and include: weak fluorescence,[51] photodetection[52,53] and liquid crystalline photoconduction.[54-57] Blatter radicals have also been incorporated in electroactive

polymers as components of purely all organic batteries.[45,58-60] It has been demonstrated that they can form stable thin films without significant degradation, while retaining their paramagnetic character.[61,62] Several recent studies[63,64] examined the Blatter radical/inorganic "spinterface" and their possible applications in spintronic devices.[65] Thin films based on Blatter-type radicals can act as metal-free spin-sources in purely organic spintronic devices.[66] Blatter radicals can also be used as polarizing agents of Overhauser DNP for high-field MAS-DNP.[67,68]

The application of Blatter radicals in cutting edge devices requires the development of "structure-activity" relationships. Such studies can help understand how intrinsic microscopic and macroscopic properties can be 'customized' to prepare materials with desired properties. Our group has focused on "structure-to-magnetism" correlations of Blatter radicals.[28-34,69-72] Herein, we present the synthesis and the magneto-structural correlation of 1,3-diphenyl-1,4-dihydrobenzo[*e*]-[1,2,4]triazin-4-yl-6,7-dicarbonitrile (**2**) a highly delocalized, electron deficient Blatter radical. The crystal structures and magnetic properties of the closely related 3-*tert*-butyl-6-cyano-1-phenyl-1,4-dihydrobenzo[*e*][1,2,4]triazin-4-yl (**3**) and 3-*tert*-butyl-7-cyano-1-phenyl-1,4-dihydrobenzo[*e*]-[1,2,4]triazin-4-yl (**4**) were previously reported by the Yoshioka group.[36] Radical **3** forms alternate 1D columns wherein the molecules are π-stacked in an antiparallel fashion with intra- and inter-dimer distances of 3.327 and 3.373 Å, respectively. This Peierl's distorted stack exhibits a reversible spin transition at *ca.* 284 K with a bistability window of 6 K. Radical **4** forms a uniform 1D column wherein the radicals overlap antiparallel mainly via the N1-phenyl substituent and the benzo[1,2,4]triazinyl moiety with intrachain distances of 3.694−3.892 Å. Radical **4** displays 1D antiferromagnetic interactions along the stacking direction with J = -15.8 cm^{-1}. These antiferromagnetic interactions are temperature independent as the distances between the radicals inside the uniform 1D chain remain approximately constant throughout the 5–300 K temperature region.

Herein, we show that radical **2** gives rise to two polymorphs (**2*α*** and **2*β***). Radicals in **2*α*** form a uniform 1D column with no evidence of Peierls' distortion despite the short interplanar distances. Pairs of radical **2** in polymorph **2*α*** demonstrate strong 1D antiferromagnetic interactions that are dependent on temperature. The magnetic susceptibility data for polymorph **2*α*** was rationalized using the *First-Principles Bottom-Up* approach.[73]

Experimental Section

See the Supporting Information for all experimental procedures (Section 1), compound characterization (Section 2), and details of the CV and EPR (Section 3), crystal packing (Section 4), powder X-ray diffraction and magnetic susceptibility measurements (Section 5), and computational methodology (Sections 6 and 7).

Results and Discussion

Synthesis

The synthesis of 1,3-diphenyl-1,4-dihydrobenzo[*e*][1,2,4]triazin-4-yl-6,7-dicarbonitrile (**2**) follows the classic synthetic route to Blatter-type radicals (see Scheme 1 and SI Section 1).[4,6,7] The structures of all intermediates (**7** to **9**) and final product (**2**) have been verified by single-crystal X-ray diffractometry (see SI Section 2).

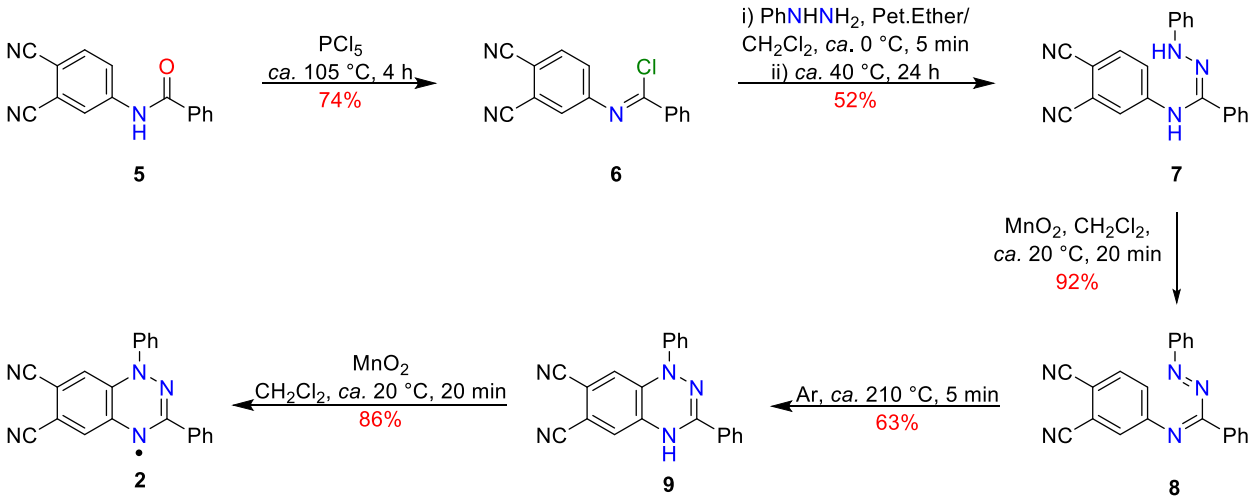

Scheme 1. Synthetic route to radical **2**.

N-(3,4-Dicyanophenyl)benzamide (**5**) and phosphorus pentachloride were heated under anhydrous conditions to *ca.* 105 °C for 4 h to afford the *N*-(3,4-dicyanophenyl)benzimidoyl chloride (**6**) in 74% yield. Reaction of the highly electrophilic benzimidoyl chloride **6** with phenylhydrazine required carefully controlled conditions to ensure reaction *via* the *α* nitrogen, and deliver *N*-(3,4-dicyanophenyl)-*N′*-phenylbenzohydrazonamide (**7**) in 52% yield. Amidrazones are electron rich and usually susceptible to oxidation. Their stability in air and on silica gel varies depending on the presence of EDG or EWG on the *N*-aryl rings. The presence of two nitrile groups stabilized amidrazone **7** towards oxidation. Amidrazone **7** crystallizes in the monoclinic space group $P2_1/c$ with one molecule in the asymmetric unit cell (see Figure S2.1 and Tables S2.1, S2.2 in SI Section 2), and participates in two weak hydrogen bonds N3-H3A···$N5_{nitrile}$ (d = 2.043 Å, ∢164.9°) and C2-H2···$N5_{nitrile}$ (d = 2.633 Å, ∢159.9°) (see Figure S2.1 for atom numbering).

Oxidation of amidrazone **7** to 4-({(*Z*)-phenyl[(*E*)-phenyldiazenyl]methylene}amino)-phthalonitrile (**8**) required an excess of a strong oxidant (MnO_2) due to its electron deficient nature owing to the presence of two nitrile groups. The resulting azoimine **8** is stable and crystallizes in the monoclinic space group $P2_1/c$ with one molecule in the asymmetric unit cell (see Figure S2.2 and Tables S2.1, S2.3 in SI Section 2), and participates in a weak hydrogen bond C6-H6···N10 (*d*

= 2.731 Å, ∢ 155.9°) (see Figure S2.2 for atom numbering). As anticipated, this oxidation leads to the reduction of the **7** amidrazone HN-C [*d* = 1.427(4) Å] and N-NH [*d* = 1.365(4) Å] bond lengths to the corresponding N=C [*d* = 1.273(5) Å] and N=N [*d* = 1.256(4) Å] of the azoimine **8** (Tables S2.2 and S2.3 in SI Section 2).

Normally the azoimine would undergo electrocyclic ring closure to the leuco triazine in the presence of DBU and Pd(C) under an atmosphere of air with high efficiency.[18] These reaction conditions failed to ring close azominine **8** due to its highly electron deficiency. Instead, a fast thermal electrocyclization for azoimine **8** was achieved at 210 °C to give the leuco form, 1,3-diphenyl-1,4-dihydrobenzo[*e*][1,2,4]triazine-6,7-dicarbonitrile (**9**), in a moderate 63% yield. Triazine **9** crystallizes in the monoclinic space group $P2_1/c$ with one molecule in the asymmetric unit cell (see Figure S2.3, S2.4 and Tables S2.1, S2.4 in SI Section 2). The triazine ring forms a characteristic half-chair structure along the N-Ph, N-H axis, typical of similar leuco triazines previously reported in the literature.[47,74-76] The folding angle between the plane of the benzo-fused moiety and the amidrazone unit is 19.22° (Figure S2.4 in SI). The nitrogen atom of the N-Ph adopts a shallow pyramidal geometry with the distance of N1 from the plane of N2, C9 and C16 at 0.182 Å (see Figure S2.3 for atom numbering). There is a significant bond localization inside the amidrazonyl moiety with N1-N2 [*d* = 1.417(2) Å] and N3-C1 [*d* = 1.390(3) Å] showing considerable single bond character and N2-C1 [*d* = 1.282(3) Å] being a typical C=N double bond. The nitriles bond lengths C14-N4 [*d* = 1.151(3) Å, ∢ 177.0(2)°] and C15-N5 [*d* = 1.142(3) Å, ∢ 178.7(3)°] are typical of C≡N triple bonds.

While conversion of electron-rich leuco triazines, to the corresponding radicals, can be achieved with base deprotonation and oxidation in air, conversion of electron-deficient leuco triazines requires the action of strong oxidants.[47] Triazine **9** treated with an excess of MnO_2 in anhydrous CH_2Cl_2 at *ca.* 20 °C for 20 min gave the desired 1,3-diphenyl-1,4-

dihydrobenzo[*e*][1,2,4]triazin-4-yl-6,7-dicarbonitrile (**2**) in 86% yield. While radical **2** showed good stability over several months at ambient conditions, it did slowly (over 12 months) revert back to the leuco form. Radical **2** was fully characterized by both solution and solid-state studies (see following sections).

Cyclic Voltammetry (CV) and Electron Paramagnetic Resonance (EPR)

The CV spectrum of radical **2** is typical of benzo[*e*][1,2,4]triazinyls with two fully reversible redox waves (Figure 2a and Figure S3.1b in SI Section 3): an oxidation (0/+1) at $E_{1/2}$ = 0.705 V and a reduction (-1/0) at $E_{1/2}$ = -0.503 V *vs* SCE with E_{cell} = 1.21 V. The introduction of two nitrile groups at the C6 and C7 positions of the benzo-fused ring dramatically reduced the reduction potential from -0.96 V of the Blatter radical **1** to -0.50 V for radical **2** and increased the oxidation potential from 0.10 V for **1** to 0.705 V for **2**.[10] This alteration reflects the electron-deficient nature of radical **2**, facilitating its easier reduction to the anion and rendering its oxidation to the cation more difficult. Solution EPR spectra for Blatter radical **1** and other benzo[*e*][1,2,4]triazinyls indicate that the spin density is primarily delocalized on the amidrazonyl fragment of the 1,2,4-triazinyl ring, as the seven-line spectrum is consistent with coupling to three nearly equivalent ^{14}N nuclei.[19-34] Further splitting is observed in radical **2**, indicating considerable delocalization of the spin density towards the nitrile groups, primarily to 7-CN and, to a lesser degree, to 6-CN. The solution EPR spectra (CH_2Cl_2, *ca.* 20 °C) of radical **2** shows coupling to five nonequivalent ^{14}N nuclei (Figure 2b and Figure S3.2 in SI Section 3). Simulation of the first-derivative mode gave g = 2.0039. The hyperfine coupling constants (hfcc) were calculated to be a_N/G = 6.66, 4.40, 2.53, 2.29, and 0.32. Previous EPR and ENDOR studies by Neugebauer on ^{15}N-labeled benzo[*e*][1,2,4]triazinyls showed that the largest ^{14}N hyperfine coupling constant (hfcc) is located at N1 followed by N4 and N2 ($a_{N1} >> a_{N4} > a_{N2}$, see Figure 1 for N numbering).[12-14] Based on these studies we can safely assign a_N/G = 6.655 to N1, and 0.319 to the N of the 6-CN group. The remaining hfcc, a_N/G = 4.40, 2.53, and 2.29, belong to N2, N4 and the N of the 7-CN group.

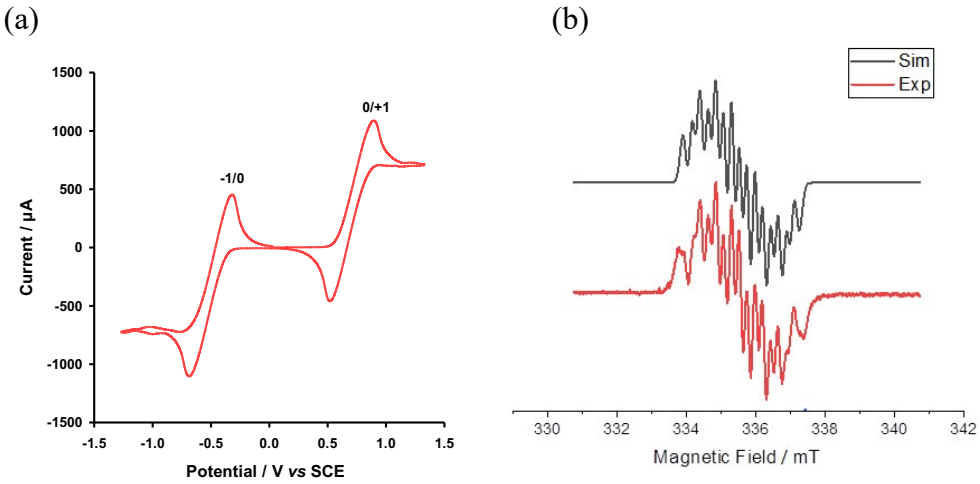

Figure 2. (a) CV of radical **2** in CH_2Cl_2 (1.0 mM); Electrolyte: *n*-Bu_4NPF_6 (0.1 M); Electrodes: Glassy C (working), Pt wire (counter) and Ag/AgCl (1.0 M KCl) (reference); Scan rate 50 mV s^{-1} Temp. 20 °C; Internal reference: Fc/Fc^+ (0.475 V *vs* SCE). (b) Experimental and simulated EPR spectra of radical **2** in CH_2Cl_2 (1 μM) at 20 °C. Fitting parameters: g = 2.0039, a_N/G = 6.66, 4.40, 2.53, 2.29, and 0.32, linewidth ΔH_{pp}/G = 2.09.

Single Crystal X-Ray Diffraction Studies

Radical **2** crystallizes in two polymorphs: ***2α*** (CCDC 2285853) and ***2β*** (CCDC 2285861). Suitable single crystals for X-ray diffraction crystallography were obtained by slow cooling of a concentrated PhMe solution for ***2α*** and CH_2Cl_2 solution for ***2β*** (Table S2.5 in SI Section 2). The crystal structures were collected at 100.00(10) K and 100(2) K for ***2α*** and ***2β***, respectively. Polymorph ***2α*** crystallizes in the orthorhombic *Pnma* space group with one molecule in the asymmetric unit cell. Polymorph ***2β*** crystallizes in the monoclinic *C2/c* space group with one molecule in the asymmetric unit cell. The volume cell size of ***2β*** [3238.5(16) $Å^3$] is twice the size that of ***2α*** [1623.53(11) $Å^3$] with eight (Z = 8) and four (Z = 4) molecules in the complete unit cell, for ***2β*** and ***2α***, respectively.

The intramolecular bond lengths and angles of polymorphs ***2α*** and ***2β*** (Figure 3 for crystallographic atom numbering and Tables S2.6 and S2.7 in SI Section 2) are similar to those of other previously reported benzotriazinyls.[27-41] Bonds N1-N2 and N3-C1 show significant double

character: d = 1.360(2) Å, 1.340(2) Å in **2*α*** and d = 1.363(2) Å, 1.344(2) Å in **2*β***, respectively. Bond N2-C1 is not a typical C=N double bond since lengthens to d = 1.333(2) Å and 1.335(2) Å in **2*α*** and **2*β***, respectively.

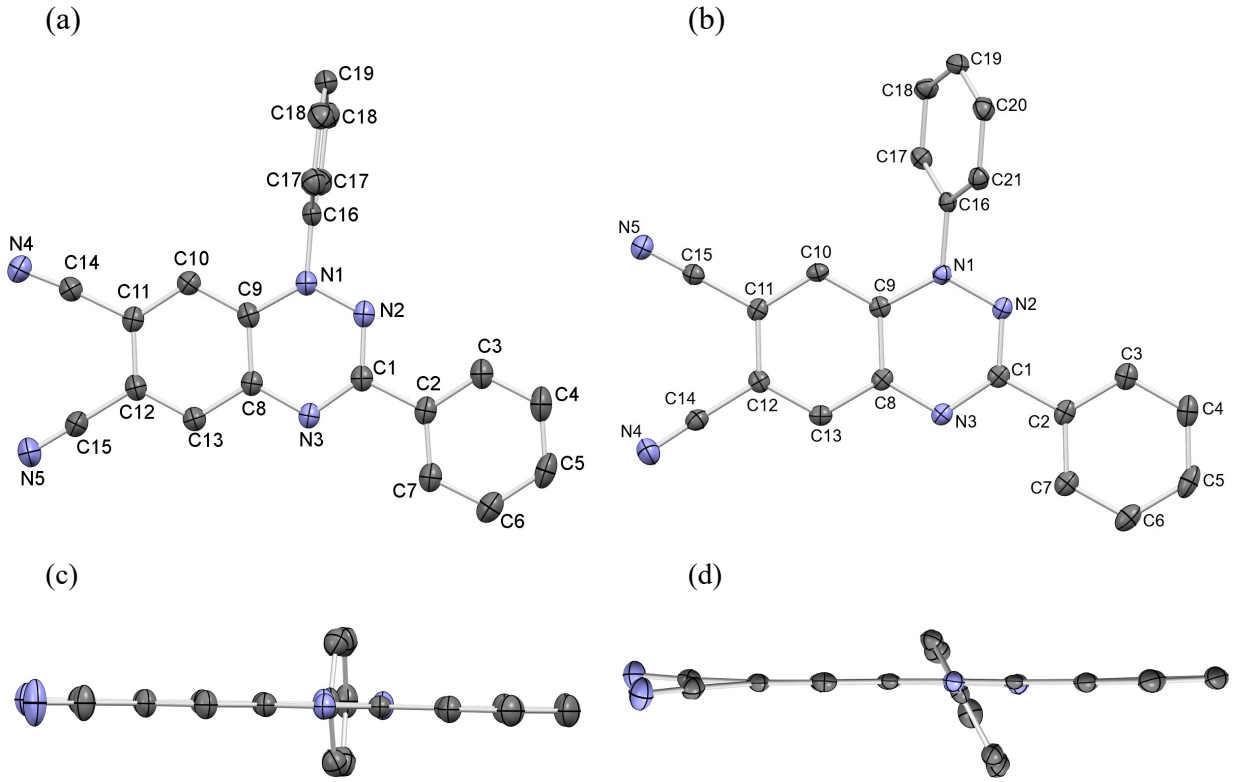

Figure 3. ORTEP view of the 1,3-diphenyl-1,4-dihydrobenzo[*e*][1,2,4]triazin-4-yl-6,7-dicarbonitrile (**2**) radical (50% probability of the thermal ellipsoids) in the crystal structure of the (a) polymorph **2*α*** and (b) polymorph **2*β*** along with the crystallographic atom numbering used in the discussion of X-ray structures. ORTEP structures viewed along the N1–N3 axis for (c) polymorph **2*α*** and (d) polymorph **2*β*** displaying the planarity of the benzotriazinyl moiety and the dihedral angle around the N-Ph substituent. Hydrogens are omitted for clarity.

The triazinyl moiety in both polymorphs is essentially planar with the distance of N1 from the plane defined by N2, C9, C16 at 0.000 and 0.059 Å for polymorphs **2*α*** and **2*β***, respectively. For polymorph **2*α*** both the benzo-fused moiety and the nitriles are in planarity with the triazinyl moiety (Figure 3c). For polymorph **2*β*** the nitriles deviate from the planarity of the benzotriazinyl moiety with the distance of N4 and N5 from the plane defined by the benzo-fused moiety (C8 to C13) at

0.190 and 0.162 Å, respectively. The torsion angle (N2, N1, C16, C17) of the N1-Ph substituent for polymorph **2*α*** is 87.78(14)°, essentially near perpendicular to the plane of the benzotriazinyl moiety. The corresponding angle for polymorph **2*β*** is 57.7(2)° which is closer to the average of 59° ± 13° previously reported for other benzotriazinyl radicals.[26-41] This torsion angle is attributed to both packing effects and the steric repulsion between the H bonded to C10 and the ortho hydrogens of the N1-Ph ring. The steric repulsion causes the subtle narrowing of angle N2-N1-C16 to 113.64(14)° in polymorph **2*α*** and 114.5(1)° in polymorph **2*β***. The C1-Ph substituent is coplanar with respect to the triazinyl moiety with torsion angle (N3, C1, C2, C7) at 0.0 and 2.0(2)° for polymorphs **2*α*** and **2*β***, respectively.

The solid-state packing in the majority of Blatter-type radicals is mainly determined by their propensity to form 1D supramolecular arrangements wherein the radicals π stack to maximize their SOMO-SOMO overlap.[26-41] This is true for both polymorphs **2*α*** and **2*β***. In polymorph **2*α***, radicals π stack antiparallel along the *b*-axis and form supramolecular one-dimensional (1D) evenly spaced chains (Figure 4). Radicals within these 1D columns are related through a center of inversion that places N1-Ph substituents on opposite sides to avoid build-up of steric hindrance and allow formation of a pair of two weak centrosymmetric hydrogen contacts C17-H17···N3 [*d* = 2.698 Å, ∢ 150.04°] that link the radicals along the 1D column (see dotted blue lines in Figure 4a-b). The interplane distance between successive radicals is 3.366 Å, which is similar to that of previously reported benzotriazinyls with near perpendicular N-Ph substituents (torsion angle ~90°).[77] Down the *b*-axis, radicals of polymorph **2*α*** overlap mainly *via* the triazinyl moieties (Figure 4c). Slippage across the *a*-axis (longitudinal slippage angle of 12.73°) places the N1 atom directly on top of the N3 atom and vice versa (Figure 4c). These two atoms hold significant spin density, which is expected to lead to a strong magnetic exchange coupling. Radicals in neighboring

1D columns are connected via a network of in-plane weak hydrogen contacts (see Figure 4d for expanded contacts of radical **2** in the asymmetric unit cell of polymorph **2*α***).

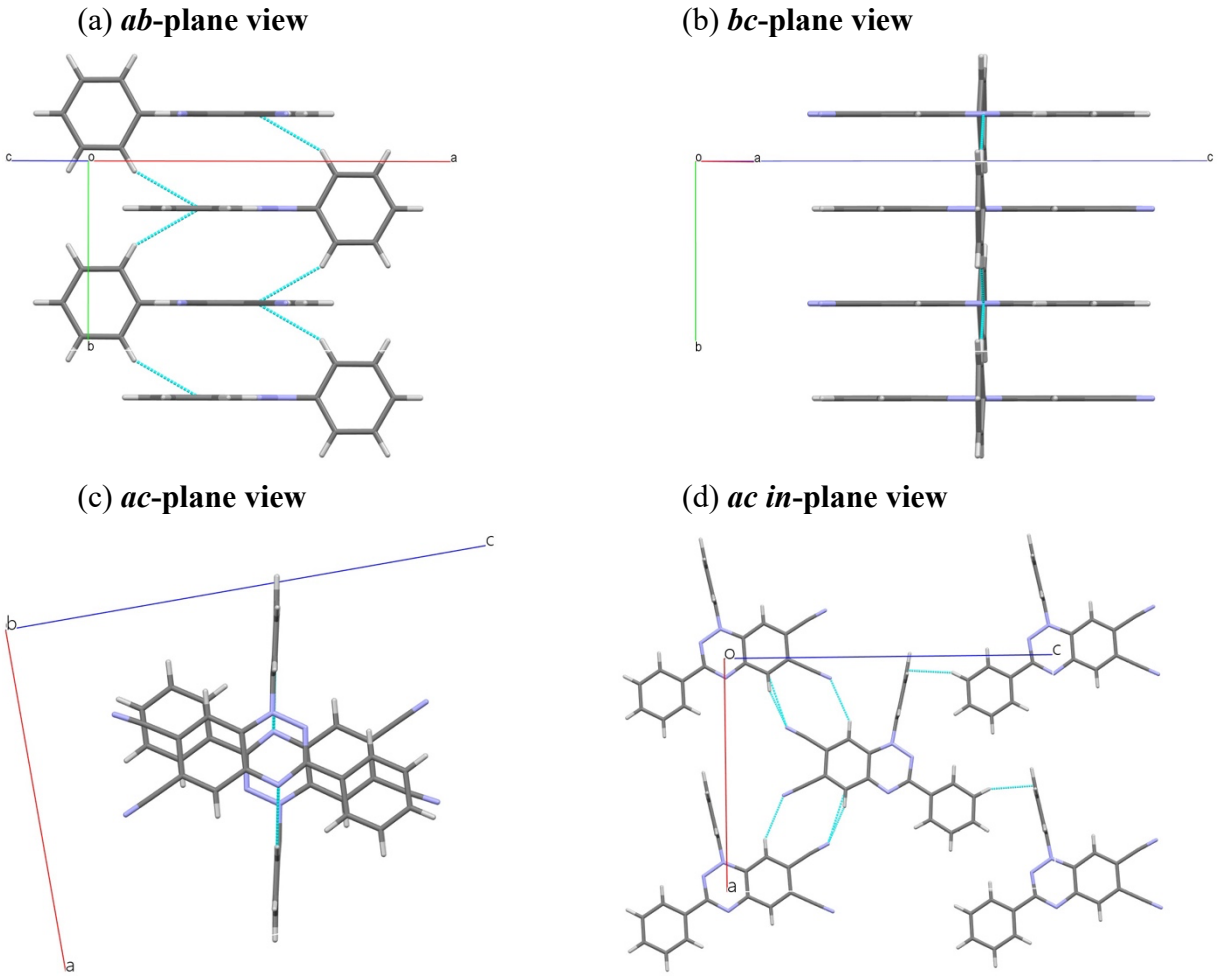

Figure 4. Supramolecular 1D chains of π-stacked radicals in polymorph **2*α*** viewed along (a) the *ab*-plane, (b) the *bc*-plane, and (c) *ac*-plane. (d) View of in-plane interactions of polymorph **2*α*** parallel to the crystallographic *ac*-plane. Shortest intermolecular contacts inside the π stacks shown in blue dotted lines.

On one side of the radical, along the *a*-axis, the nitrile groups form two centrosymmetric H-bonds C14-N4···H13 [d = 2.306 Å, ∡ 160.2°] and C15-N5···H10 [d = 2.710 Å, ∡ 152.4°]. On the other side, along the *c*-axis, there is an edge-to-face (Y-shaped geometry) $\pi\cdots\pi$ stacking interaction between the C1-Ph and N1-Ph substituents with one close contact, namely, C4-

H4···C19 d = 2.586 Å (Figure 4d). In-plane interactions lead to the formation of 2D sheets that pack parallel to the *b*-axis and form a tight three-dimensional packing without any voids (Figure S4.1 in SI)

The subtle changes in the intramolecular geometry of polymorph **2*β*** have significant consequences in its crystal-packing (see SI Section 4). Contrary to the 1D regular chains of **2*α***, in polymorph **2*β***, radicals form 1D alternate chains due to two distinct dimers (I and II in Figure 5a) whose interplane distances are 3.182 and 3.318 Å, respectively. Remarkably, radicals inside the alternate 1D chains of polymorph **2*β*** are also arranged in a centrosymmetric pattern, placing the N1-Ph substituents on opposite sides (Figure 5a) and overlapping mainly *via* their triazinyl moieties (Figure 5b), as in polymorph **2*α***.

Polymorph **2*β*** could then potentially be the outcome of an applied Peierls distortion to the 1D regular chains of polymorph **2*α***, as observed in many related 1D spin systems,[78-83] leading to alternation of dimerized I pair and non-dimerized II pair of radicals in **2*β***. Considerable spin pairing is to be expected due to both (i) the close proximity of the radicals within both I and II pairs, which gives rise to a rich network of contacts (see blue dotted lines in Figures 5a), and (ii) triazinyl moieties superimposing (see N1 of one radical on top of atom N3 of the other radical in Figure 5b). Therefore, multiple pathways for antiferromagnetic coupling can be potentially anticipated. Finally, neighboring 1D columns are connected by in-plane weak hydrogen contacts via nitrile groups C13-H13···N5 [d = 2.424 Å, ∢ 162.3°, Figure 5c] and by H···H interactions between nearby N1-Ph substituents H18···H18 [d = 2.229 Å, Figure 5c].

(a) ***ac*-plane view** (b) ***ab*-plane view** (c) ***ab in*-plane view**

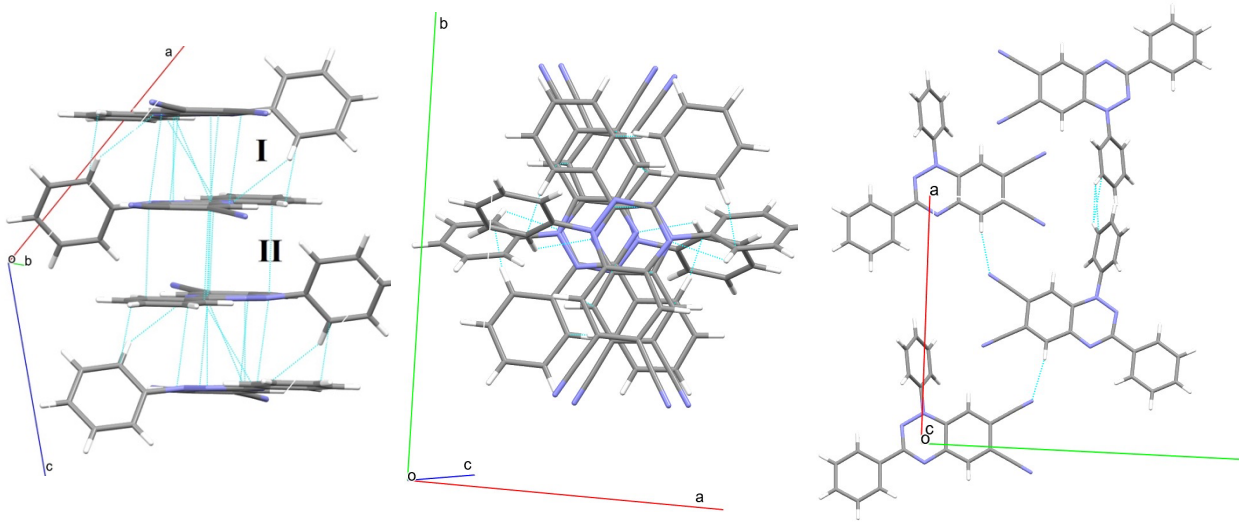

Figure 5. Supramolecular 1D chains of π-stacked radicals in polymorph **2*β*** viewed along (a) the *ac*-plane, and (b) *ab*-plane. (c) View of in-plane interactions of polymorph **2*β*** perpendicular to the crystallographic *ab*-plane. Shortest intermolecular contacts inside and between π stacks shown in blue dotted lines.

Magnetic Susceptibility Measurements

Before measuring the magnetic properties of polymorphs **2*α*** and **2*β***, we collected analytical data to confirm their chemical purity as well as their powder X-ray diffraction patterns to confirm phase purity. Despite our best efforts we were unable to secure a phase pure sample of polymorph **2*β*** for magnetic susceptibility studies. From hereon we focus on the magnetic properties of polymorph **2*α***. The experimental diffraction signature of a polycrystalline sample of **2*α*** closely matched the pattern calculated from single crystal X-ray structure at 100(2) K supporting phase purity (Figure S5 in SI Section 5). However, the presence of small amounts of amorphous paramagnetic impurities cannot be fully excluded.

We have measured the temperature dependence of the magnetic susceptibility (χ) on a polycrystalline sample of **2*α*** in an applied field of 0.5 T, in the 2-300 K temperature region (see $\chi(T)$ and $\chi T(T)$ in Figures 6a and 6b, respectively). Paramagnetic susceptibility data (χ) were

collected in both warming and cooling modes with no apparent differences. Data were corrected for the sample holder, intrinsic diamagnetic contributions, and temperature independent paramagnetism (see SI Section 5 for details).

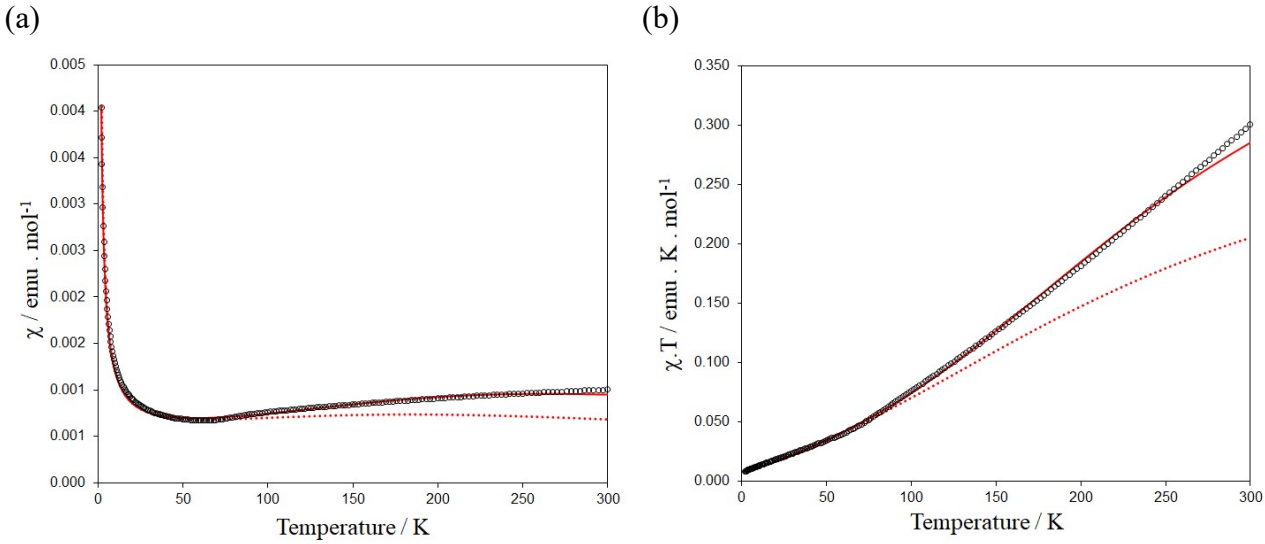

Figure. 6 (a) Temperature dependence of the magnetic susceptibility χ, and (b) the χ*T* product for polymorph **2*α*** at 0.5 T in 2–300 K range (χ is defined as *M*/*H* per mole of radical **2**). The red dotted lines are the fit of the experimental data to the simple regular chain model of antiferromagnetically coupled quantum spins developed by Bonner and Fisher (BF).[84-86] The red solid lines are the best fit of the experimental data in the amended temperature-dependent BF model; see text for details.

The χ*T* product for polymorph **2*α*** at 300 K is 0.3 emu K mol^{-1} (Figure 6b), which is significantly smaller than the expected Curie constant of 0.375 emu K mol^{-1} for an $S = 1/2$ spin with a *g* factor of ~2. This divergence indicates strong antiferromagnetic interactions between the radicals. This is further supported by the broad peak of the molar susceptibility (seen as a plateau in the χ *vs T* plot, Figure 6a), which gradually decreases upon cooling from 300 K down to 70 K. The rise in susceptibility below 50 K is attributed to a Curie-tail stemming from paramagnetic lattice defects, *i.e.*, uncoupled radicals.

Following our previous crystal packing analysis of polymorph **2*α***, we tentatively assigned the strongest antiferromagnetic interactions along the 1D regular chain of radicals down the *b*-axis

(Figure 4). Accordingly, the appropriate model to fit the magnetic data of polymorph **2*α*** was expected to be Bonner and Fischer's (BF) analytical expression established in 1964,[84-86] that accounts for a regular chain of $S = 1/2$ quantum spins with a single magnetic fitting parameter, J, between radical centers (BF uses as Hamiltonian: $\widehat{H} = -\sum_{A}^{N-1}\sum_{B>A}^{N} J_{AB}\,\hat{S}_A \cdot \hat{S}_B$, where A, B are different radicals).

Attempts to model the experimental magnetic data using the BF regular chain model over the whole temperature range (2–300 K) were, nevertheless, unsuccessful. A satisfactory fit could be achieved in the 2–80 K range (red dotted line in Figure 6) with fitting parameters J/k = -310 K (-215.5 cm^{-1}), ρ = 0.981, *i.e.*, 1.9% lattice defects – curie tail, and g = 2.0039 as determined by EPR. However, the steeper rise in the magnetic susceptibility (χ) above 80 K could not be rationalized using the BF model. Normally the J magnetic exchange fitting parameter in BF model is considered to be independent of temperature, which is true when the thermal expansion of the crystal lattice does not cause significant changes in the intermolecular distances and/or interactions responsible for the observed macroscopic magnetic properties. Yet, the actual J_{AB} exchange coupling depends on the overlap between radicals, and therefore any changes in the crystal lattice that cause alterations in the intermolecular separation along the stacking direction will directly affect the observed magnetic susceptibility (χ).

Effect of temperature on the crystal packing and magnetism of 2*α*

Building on previous both experimental[33] and computational experience,[87-89] we anticipated that increasing interplanar distances along the *b*-axis in the 1D chains of **2*α*** led to a weaker J_{AB} magnetic exchange coupling and an increase in the observed paramagnetism. As such, we performed a variable-temperature (VT) X-ray diffraction study to examine the effect of temperature on the intermolecular geometrical parameters in the crystal lattice of polymorph **2*α***. X-ray diffraction data were collected on the same crystal at 80 (CCDC 2285930), 100 (CCDC 2285853), 150 (CCDC

2285854), 200 (CCDC 2285855), 250 (CCDC 2285857) and 300 K (CCDC 2285858) and structures were fully solved (see SI Section 4 for data, and Table 1 for main geometrical parameters of polymorph **2*α*** in the temperature range of 80–300 K).

There is an increasing trend in the cell dimensions of polymorph **2*α*** ongoing from 80 to 300 K apart from an anomalous decrease in *a* and *c* at 100 K. The intramolecular geometrical parameters of radical **2** in polymorph **2*α*** remain essentially the same throughout the 80–300 K range (see Table S4.1 in SI Section 4). The intermolecular contacts and the interplane separation of the radicals in **2*α*** undergo a subtle but significant increase (Table 1).

Two of these intermolecular contacts experience a greater increase in their length: (i) the hydrogen bond linking radicals inside the 1D column C17-H17···N3 increases from d = 2.700 Å at 80 K to 2.812 Å at 300 K representing ~4% increase; and, (ii) one of the two centrosymmetric nitrile hydrogen bonds connecting neighboring stacks C15-N5···H10 increases from d = 2.705 Å at 80 K to 2.837 Å at 300 K representing a ~5% increase. In terms of the observed increase in the paramagnetism of polymorph **2*α*** above 80 K, the interplane distances along the stacking direction increase from 3.3641(2) Å at 80 K to 3.4500(3) at 300 K, *i.e.*, a 2.6% increase that coincides with the 2.6% increase of the unit cell *b*-axis.

Opening of the gap between the radicals inside the 1D column by an overall 0.086 Å indicated that J_{AB} cannot be held constant, as the overlap between radicals diminishes, and was therefore temperature dependent. The change in the magnitude of the J_{AB} exchange interaction with temperature owing to thermal expansion (contraction) of the crystal as temperature increased (decreased), was named as *exchange elasticity* by O. Kahn,[90] and has been previously reported for other paramagnetic materials.[33,91-95]

Table 1. Geometrical parameters of polymorph **2*α*** determined at 80, 100, 150, 200, 250 and 300 K. The VT-X-ray diffraction study was performed on the same crystal.

Temperature (K)	80	100	150	200	250	300
Space Group	Pnma Orthorhombic					
a, Å	13.0948(7)	13.0900(5)	13.1222(6)	13.1460(7)	13.1789(8)	13.2231(10)
b, Å	6.7282(5)	6.7329(3)	6.7687(3)	6.8054(4)	6.8475(5)	6.9000(6)
c, Å	18.4238(9)	18.4213(7)	18.4344(8)	18.436(1)	18.4400(12)	18.4336(16)
V, Å^3	1623.22(16)	1623.53(11)	1637.34(13)	1649.36(16)	1664.07(19)	1684.6(2)
Intrachain intermolecular contacts (Å)						
Interplane distance=*b*/2	3.3641(2)	3.3665(2)	3.3844(2)	3.4027(2)	3.4238(2)	3.4500(3)
N1…N3	3.440	3.442	3.462	3.483	3.507	3.536
H17…N3	**2.700**	**2.698**	**2.719**	**2.742**	**2.775**	**2.812**
C9…C1	3.464	3.467	3.487	3.509	3.531	3.561
N2…C8	3.445	3.448	3.468	3.488	3.512	3.541
C8…C1	3.417	3.418	3.434	3.449	3.468	3.491
Interchain intermolecular contacts (Å)						
N4…H13	2.305	2.306	2.322	2.331	2.349	2.372
N5…H10	**2.705**	**2.710**	**2.737**	**2.765**	**2.801**	**2.837**
C19…H4	2.583	2.586	2.594	2.600	2.623	2.645

A temperature dependent magnetic exchange *J* parameter was, therefore, included in the BF model to account for the coupling between changes in the crystal volume and the actual J_{AB} exchange interaction in **2*α***. After exploring different possibilities (see SI Section 4), incorporating the phenomenological quadratic expression $\left|J_{fit}/k\right| = |J/k| - 0.0018T^2$ into the BF fitting model accounted for the steeper rise in paramagnetism at the 80–300 K temperature region (where $|J/k|$ = 310 K from the temperature-independent BF model). The coefficient accompanying the T^2 term was obtained after fitting the magnetic susceptibility data (χ) using the temperature-dependent BF model (red solid line in Figure 6, which yields a very good fit across the 2–300 K temperature region). Using the empirical expression, $\left|J_{fit}/k\right| = 310 - 0.0018T^2$ K, the value of the magnetic exchange coupling was estimated at different temperatures for **2*α*** (see J_{fit} in cm^{-1} in Table 2).

To reproduce the magnetic susceptibility experimental data of **2*α*** from *ab initio* calculations, we screened a variety of functionals and basis sets to assess which agreed best with

the values estimated for the magnetic exchange interaction obtained by fitting the BF model with $|J_{fit}/k| = 310 - 0.0018T^2$ to experimental χ(T) data (see SI Section 6 for full details). J_{comp} magnetic couplings were calculated using a pair of radicals extracted from the π stack of the crystal geometries acquired at temperatures ranging from 80 to 300 K to be able to compare them to J_{fit} from the BF modified model.

Table 2. Experimental and calculated magnetic exchange coupling interactions (in cm^{-1}) of **2*α***.*

			J_{comp} at UB3LYP (cm^{-1})				
			J_π	J_π	J_π	J_π	$J_{\pi,nn}$
T (K)	d_{ip} (Å)	J_{fit} (cm^{-1})	def2-TZVP	6-311G(d,p)	6-31G(d)	6-31+G(d)	
80	3.3641(2)	−207.4	−174.2	−198.9	–184.9	–199.0	–4.4
100	3.3665(2)	−202.9	−172.1	−196.9	–182.8	–197.4	–4.4
150	3.3844(2)	−187.3	−160.9	−184.0	–170.7	–184.0	–3.8
200	3.4027(2)	−165.4	−147.5	−169.1	–156.7	–169.2	–3.4
250	3.4238(2)	−137.3	−134.1	−154.1	–142.4	–154.4	–3.0
300	3.4500(3)	−102.9	−117.7	−136.0	–125.2	–136.0	–2.4

* Experimental *J* estimated using the temperature amended exchange interaction $|J_{fit}/k| = 310 - 0.0018T^2$ in K, and computationally calculated J_{comp} at UB3LYP level using different basis sets [namely, def2-TZVP, 6-311G(d,p), 6-31G(d) and 6-31+G(d)] at various temperatures (T in K). Interplane distance, which corresponds to *b*/2, is also given (d_{ip} in Å) for each temperature.

Among all functionals, magnetic couplings calculated at unrestricted UB3LYP level (J_{comp}) compare well with J_{fit}. In regard to basis sets (see Table 2), the 6-31+G(d) provided the optimal calculated exchange interaction by balancing good performance at both low and high temperatures. Note that def2-TZVP data actually overlap with the experimental curve at 250 K but performed poorly at low temperatures. Therefore, all remaining simulations to reproduce the magnetic susceptibility experimental data of **2*α*** from *ab initio* calculations were carried out at UB3LYP/6-31+G(d) level of computation.

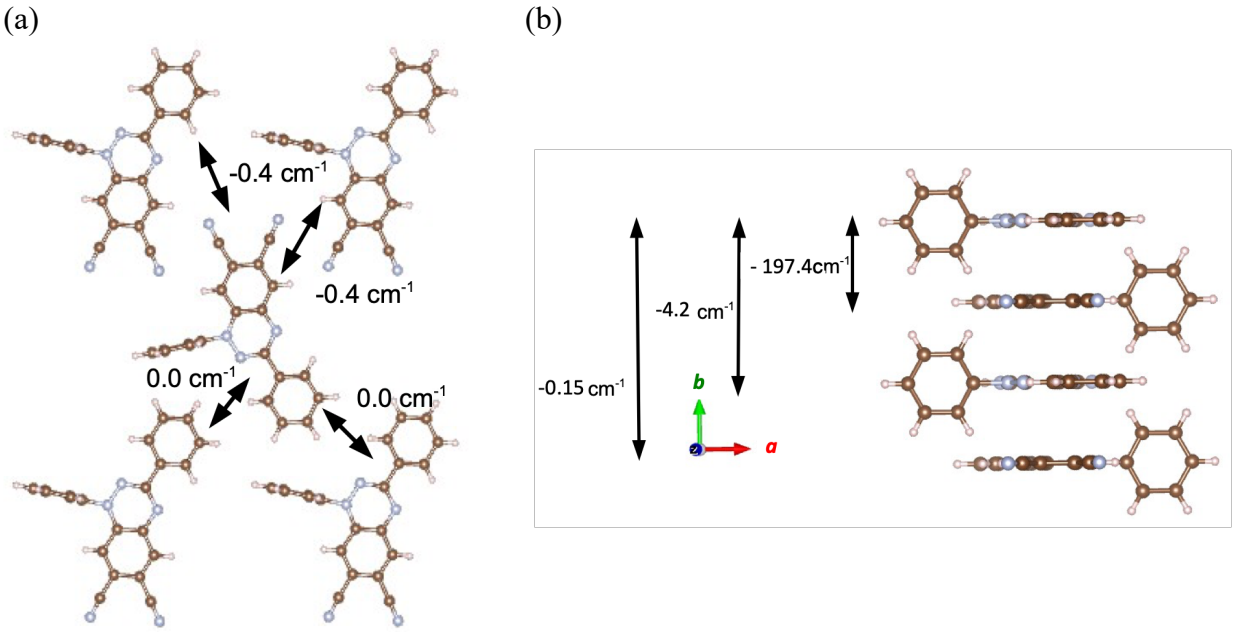

Figure 7. (a) Lateral radical···radical contacts in *ac*-plane with corresponding J_{AB} interactions, and (b) π-stacking J_{π} = -197.4 cm^{-1} (*b*-axis) with calculated nearest neighbor $J_{\pi,nn}$ = -4.2 cm^{-1}, and next-nearest neighbor $J_{\pi,nnn}$ = -0.15 cm^{-1} using a dimer and 4-radical models, respectively. All J_{AB} magnetic couplings in cm^{-1}.

As for explaining why J_{comp} decreased upon temperature increase, one must pay attention to the fact that, as the crystal lattice expands at higher temperatures, the radicals within the 1D regular chain begin to move apart. Their SOMO-SOMO overlap reduces and the magnitude of the exchange coupling interaction is cut by almost half, *ca.* 100 cm^{-1} (Table 2), for an increase of 0.086 Å in the interplane distance. As a result of a weaker magnetic exchange coupling along the 1D chain, we have a steeper increase in the samples' paramagnetism > 80 K.

Reproducing the magnetic susceptibility experimental data of 2*α* computationally

Prior to calculation of the magnetic response of polymorph **2*α*** by means of our first-principles bottom-up working strategy,[96,97] analysis of the crystal packing of **2*α*** measured at different temperatures provided pairs of radicals most likely to feature a non-negligible J_{AB} magnetic coupling

(unbiased selection criteria are distance between spin-carrying atoms within the radicals). Along the π stack one can envisage J_{π}, $J_{\pi,nn}$, and $J_{\pi,nnn}$ between neighboring radicals, and between nearest, and next-nearest neighbors, respectively, whose magnetic interactions should be evaluated (see Figure 4a). In addition, pairs of radicals in the *ac*-plane (see Figure 4d) might also be relevant candidates to interpret the magnetic response of **2*α*** and, thus, their associated J_{AB} should be assessed. At 100 K, all the *ac*-plane lateral couplings (see 0.0 and -0.4 cm^{-1} in Figure 7a) as well as nearest and next-nearest neighbor interactions (see -4.2 and -0.3 cm^{-1} in Figure 7b) were negligible compared to J_{π} between neighboring radicals along the π-stacking (-197.4 cm^{-1}).

This very same image is encountered at all temperatures. Accordingly, the magnetic topology consists of isolated AFM chains. A cyclic 16-radical AFM chain model has been used to calculate the magnetic susceptibility data (see SI Section 7 for further details), whose χT product required a temperature of about 2000 K to reach the limiting value of 0.375 emu K mol^{-1} (note it has been previously reported to be 0.3 emu K mol^{-1} for polymorph **2*α*** at 300 K, see Figure 6b).

The experimental magnetic susceptibility χ(T) data was finally reproduced for temperatures above 50 K using cyclic AFM chain models with the J_{π} and $J_{\pi,nn}$ magnetic couplings computed using geometries extracted from the crystal data characterized at different temperatures (see Table 2) (namely, 80 K in red, 100 K in green, 150 K in cream, 200 K in brown, 250 K in blue and 300 K in grey in Figure 8a). At low temperatures, fitting of the experimental data to a modified BF model hints at the presence of 1.9% of uncoupled radicals in the crystalline sample. We proceeded to simulate the existence of radicals within the cyclic AFM chain model by not letting one radical to antiferromagnetically couple to adjacent neighbor radicals (see SI Section 7 for further discussion). The contribution of those uncoupled radicals (see empty purple symbols in Figure 8a) rationalized quantitatively the experimental χ(T) data below 50 K. Yet the percentage of free radicals decreased as temperature increased (see empty purple symbols in Figure 8b). Our calculations show that there

are a 1.9% of uncoupled radicals at T < 20.5 K, which reduced to 1.5% at 28 K and further to 1.0% at 35.5 K. At 45.5 K, the number of free radicals was < 0.5% and becomes negligible at 63 K, temperature at which the X-ray data at 80 K clearly reproduced the experimental data.

In addition to magnetic susceptibility as a function of temperature, magnetization was calculated as a function of magnetic field at 2, 60, 100 and 300 K (see Figure 9a and 9b for comparison between experimental and calculated data, respectively). Interestingly, the calculated data at 2 K using the cyclic AFM chain model showed basically zero magnetization (solid brown), which was to be expected since at 2 K only the singlet ground state must be populated. As temperature increases from 60 to 100 to 300 K, higher spin multiplicity states, *i.e.*, $S \neq 0$, get populated and thus magnetization showed signal.

Our calculated $M/M_{sat}(H)$ at 2 K data (solid brown symbols in Figure 9b) differed from the experimental data because our cyclic magnetic model had no defects and, therefore, there were no free radicals. Using the previous magnetic model to simulate the presence of uncoupled radicals, the experimental $M/M_{sat}(H)$ response at 2 K was again reproduced. Indeed, even the ratio between $M/M_{sat}(H)$ at 2 and 300 K was replicated (see solid and empty brown symbols to be compared to solid orange circles in Figure 9a and 9b, respectively). Note also that the calculated response at 60 and 100 K was larger than experimentally observed.

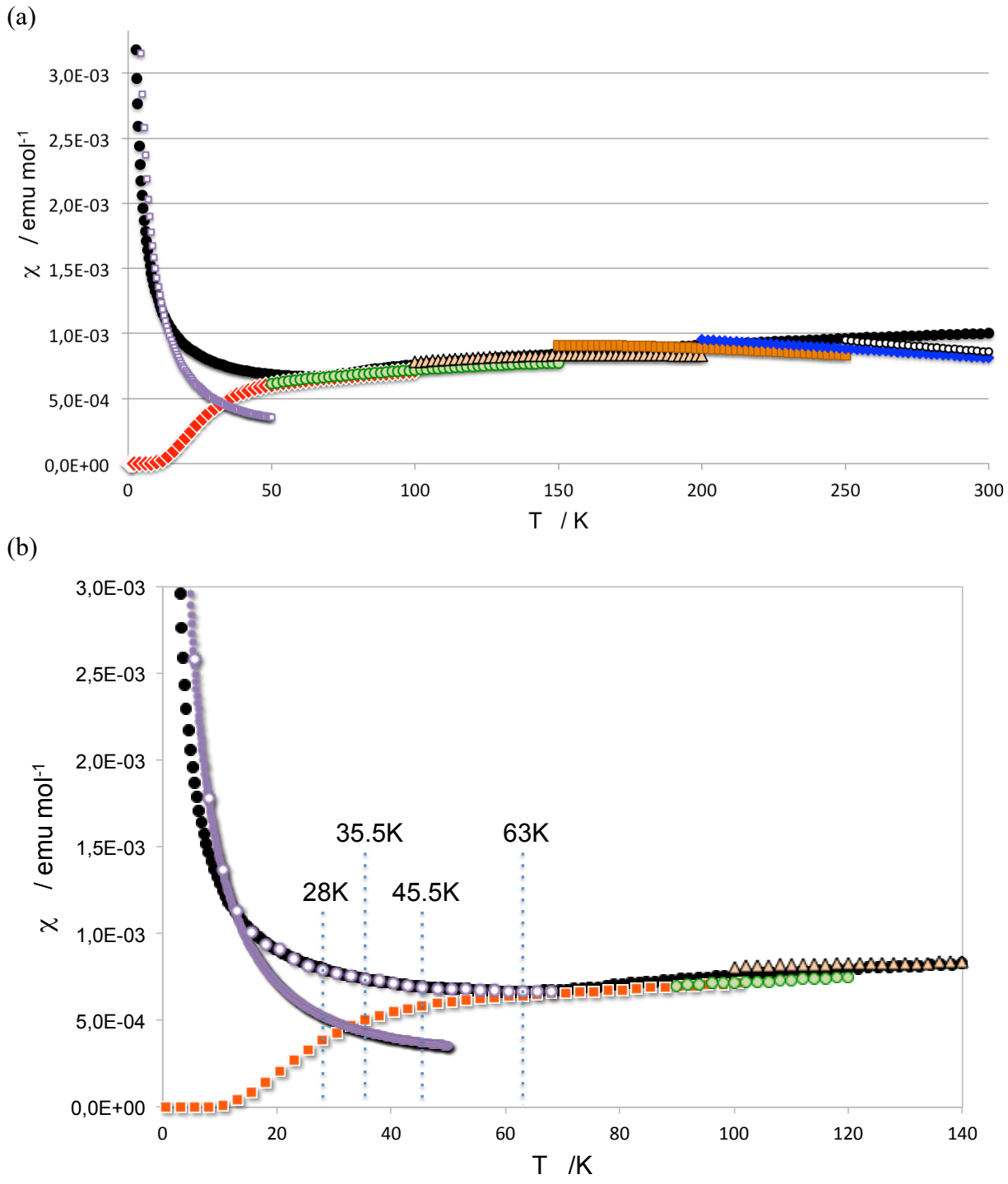

Figure 8. (a) Comparison between experimental (in black) and calculated χ(T) magnetic susceptibility using a 16-radical cyclic chain AFM model with J_{AB} values listed in Table 2. Data using geometries extracted from X-ray crystallographic data characterized at 80 K (red), 100 K (green), 150 K (cream), 200 K (brown), 250 K (blue) and 300 K (grey). See also calculated χ(T) using a modified cyclic chain AFM model to account for uncoupled radicals (purple) with J_{AB}

values using geometries extracted from X-ray crystallographic data characterized at 80 K. (b) See main text for percentages of free radicals required to reproduce the experimental χ(T) data.

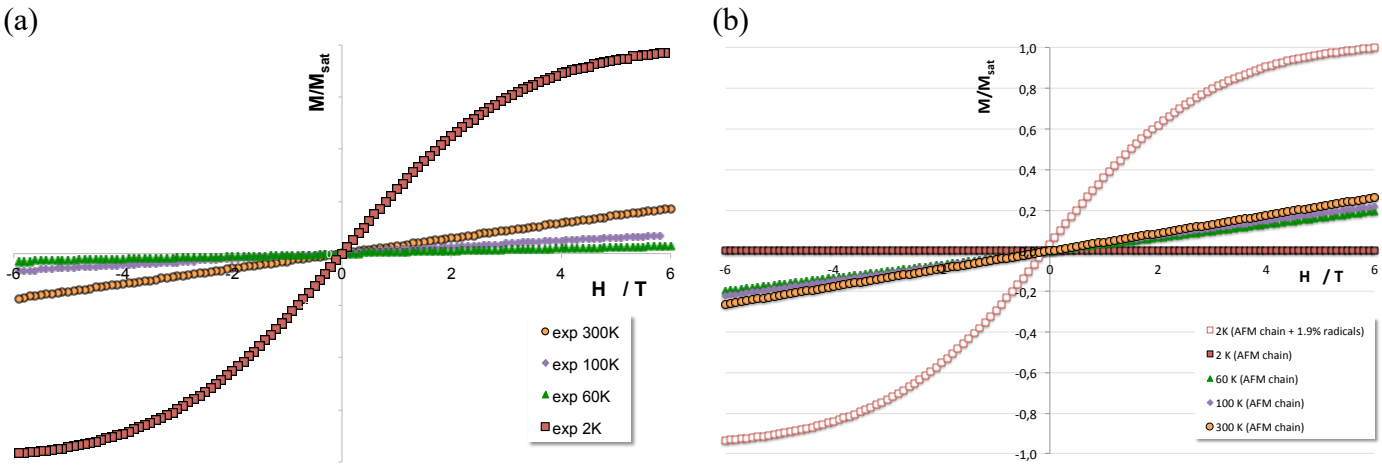

Figure 9. Comparison between (a) experimental and (b) calculated $M/M_{sat}(H)$ magnetization. A 16-radical cyclic AFM chain model with computed J_{AB} couplings from geometries extracted from X-ray 80 K was used to calculate magnetization at 2 K (solid brown), 60 K (green), 100 K (purple) and 300 K (orange). A modified cyclic chain AFM model to account for uncoupled radicals was also used to calculate magnetization at 2 K (empty brown).

The computational analysis of **2*α*** provided a sound interpretation of the magnetic response of the material in terms of magnetic susceptibility and magnetization. The 1D magnetic topology expected from direct observation of the crystal packing was corroborated. Interestingly, the magnetic exchange interaction between *π*-stacked dicyanobenzotriazinyl radicals was tuned by the temperature itself, which should be profited from if these radicals were offered as building blocks for electronic and spintronic applications.

Conclusions

1,3-Diphenyl-1,4-dihydrobenzo[*e*][1,2,4]triazin-4-yl-6,7-dicarbonitrile (**2**) is a stable electron deficient organic radical with a promising potential to be used as a building block in a range of electronic and spintronic materials. Two polymorphs, **2*α*** and **2*β***, have been identified and

characterized by single crystal X-ray diffractometry. Crystal analysis shows that, evenly packed radicals (at 3.366 Å interplanar distances) that form 1D π stacks in polymorph **2*α***, locate at alternate interplanar distances (3.182 Å and 3.318 Å) in the 1D π stack for polymorph **2*β***. Magnetic susceptibility measurements for polymorph **2*α*** indicate strong antiferromagnetic interactions along the 1D regular chain. Magnetic susceptibility data can only be fully fitted to a modified Bonner and Fischer model, which must include a temperature-dependent AFM exchange parameter within the 1D π stacks.

The computational analysis of the alpha polymorph of the title compound (***2α***) sustains that the significant magnetic couplings run along the π-stacked dicyanobenzotriazinyl radicals (J_π). Accordingly, the magnetic topology of this compound consists of isolated AFM chains. The J_π magnetic interaction is highly dependent on the temperature at which the crystal data is characterized, ranging from -136.0 cm^{-1} at 300 K to -199.0 cm^{-1} at 80 K. Numerical values of J_π couplings have been validated against both DFT and wavefunction calculations. It thus follows that, to reproduce the experimental χ(T) magnetic susceptibility data, one must account for all the changes that the J_{AB} magnetic interactions undergo upon cooling from 300 to 80 K (or upon heating from 80 to 300 K). This means that the same model with as many sets of J_{AB} couplings as experimental sets of X-ray data should be used to calculate χ(T). At low temperatures (T < 50 K), it is necessary to introduce the presence of 1.9% of uncoupled radicals to reproduce the experimental χ(T) data (note the number of uncoupled radicals becomes negligible at T > 50 K). Also, the presence of free radicals is required to rationalize the experimental $M/M_{sat}(H)$ response at 2 K since, if no defects are present in the cyclic chain AFM model, the response would show no signal (the only state populated would be the singlet ground state). The observed magnetization at higher temperatures (namely, 60, 100 and 300 K) can be fully understood in terms of higher spin

multiplicity states, *i.e.*, $S \neq 0$, that get populated upon heating. Our experimental as well as computational results reveal that temperature is the key to rationalizing the magnetism in **2*α***.

Associated Content

SI Supporting Information

Synthesis of molecules **2, 6-9**; single crystal X–ray diffractometry studies; cyclic voltammetry (CV) and electron paramagnetic resonance (EPR) of molecule **2**; crystal packing of polymorphs **2*α*** and **2*β***; powder X–ray diffraction and magnetic susceptibility measurements for molecule **2**; computational methodology; first-principles bottom-up approach analysis of **2*α***.

Accession Codes

CCDC 2285850-2285930 contain the supplementary crystallographic data for this paper. These data can be obtained free of charge via www.ccdc.cam.ac.uk/data_request/cif, or by emailing data_request@ccdc.cam.ac.uk, or by contacting The Cambridge Crystallographic Data Centre, 12 Union Road, Cambridge CB21EZ, UK; fax: +44 1223336033.

Acknowledgements

The authors thank Prof. Jeremy M. Rawson, University of Windsor for early discussions. C. P. Constantinides thanks the University of Michigan-Dearborn for an UM-Dearborn Scholars award. P. A. Koutentis and G. A. Zissimou thank the ONISILOS MSCA COFUND Fellowship Programme - Grant Agreement No 101034403, the A. G. Leventis Foundation for helping to establish the NMR facility at the University of Cyprus, the Cyprus Research Promotion Foundation and the following organizations and companies in Cyprus for generous donations of chemicals and glassware: the State General Laboratory, the Agricultural Research Institute, the Ministry of Agriculture, MedoChemie Ltd., Medisell Ltd., Biotronics Ltd. M.D. and J.R.-A. are thankful for the financial support of the Spanish Ministerio de Ciencia e Innovación (Project PID2020-117803GB-I00), and the Generalitat de Catalunya (Project 2021SGR00354).

Conflicts of interest

The authors declare no conflicts of interest.

References

1. Hicks, R. G. (Ed.), *Stable Radicals: Fundamentals and Applied Aspects of Odd-Electron Compounds*, John Wiley & Sons Ltd, Wiltshire, **2010**.
2. Hicks, R. G. What's new in stable radical chemistry? *Org. Biomol. Chem.* **2007**, *5*, 1321-1338.
3. Forrester, A. R.; Hay, J. M.; Thomson, R. H. *Organic Chemistry of Stable Free Radicals*, Academic Press, London, **1968**.
4. Constantinides, C. P.; Koutentis, P. A. Stable N- and N/S-Rich Heterocyclic Radicals: Synthesis and Applications. *Adv. Heterocycl. Chem.* **2016**, *119*, 173-207.
5. Rajca, A. Organic Diradicals and Polyradicals: From Spin Coupling to Magnetism? *Chem. Rev.* **1994**, *94*, 871-893.
6. Ji, Y.; Long, L.; Zheng, Y. Recent advances of stable Blatter radicals: synthesis, properties and applications. *Mater. Chem. Front.* **2020**, *4*, 3433-3443.
7. Rogers, F. J. M.; Norcott, P. L.; Coote., M. L. Recent advances in the chemistry of benzo[*e*][1,2,4]triazinyl radicals. *Org. Biomol. Chem.* **2020**, *18*, 8255-8277.
8. Kumar, S.; Kumar, Y.; Keshri, S. K.; Mukhopadhyay, P. Recent Advances in Organic Radicals and Their Magnetism. *Magnetochemistry* **2016**, *2*, 42.
9. Gallagher, N. M.; Bauer, J. J.; Pink, M.; Rajca, S.; Rajca, A. High-Spin Organic Diradical with Robust Stability. *J. Am. Chem. Soc.* **2016**, *138*, 9377-9380.
10. Constantinides, C. P.; Koutentis, P. A.; Krassos, H.; Rawson, J. M.; Tasiopoulos, A. J. Characterization and Magnetic Properties of a “Super Stable” Radical 1,3-Diphenyl-7-trifluoromethyl-1,4-dihydro-1,2,4-benzotriazin-4-yl. *J. Org. Chem.* **2011**, *76*, 2798-2806.

11. Blatter, H. M.; Lukaszewski, H. A new stable free radical. *Tetrahedron Lett.* **1968**, *9*, 2701-2705.

12. Neugebauer, F. A.; Umminger, I. Über 1,4-Dihydro-1,2,4-benzotriazinyl-Radikale. *Chem. Ber.* **1980**, *113*, 1205-1225.

13. Neugebauer, F. A.; Umminger, I. 1,4-Dihydro-1,2,4-benzotriazin-Radikalkationen. *Chem. Ber.* **1981**, *114*, 2423-2430.

14. Neugebauer, F. A.; Rimmler, G. ENDOR and triple resonance studies of 1,4-dihydro-1,2,4-benzotriazinyl radicals and 1,4-dihydro-1,2,4-benzotriazine radical cations. *Magn. Reson. Chem.* **1988**, *26*, 595-600.

15. Kadirov, M. K.; Il'yasov, A. V.; Vafina, A. A.; Buzykin, B. I.; Gazetdinova, N. G.; Kitaev, Y. P. Double electron-nuclear resonance of free radical 1,3-diphenyl-1,4-dihydro-1,2,4-benzotriazin-4-yl. *Bull. Acad. Sci. USSR, Div. Chem. Sci.* **1984**, *33*, 649-650.

16. Mukai, K.; Inoue, K.; Achiwa, N.; Jamali, J. B.; Krieger, C.; Neugebauer, F. A. Magnetic-properties of 1,4-dihydro-1,2,4-benzotriazin-4-yl radicals. *Chem. Phys. Lett.* **1994**, *224*, 569-575.

17. Hutchison, K. A.; Srdanov, G.; Menon, R.; Gabriel, J.-C. P.; Knight, B.; Wudl, F. A Pressure Sensitive Two-Dimensional Tetracyanoquinodimethane (TCNQ) Salt of a Stable Free Radical. *J. Am. Chem. Soc.* **1996**, *118*, 13081-13082.

18. Koutentis, P. A.; Lo Re, D. Catalytic Oxidation of *N*-Phenylamidrazones to 1,3-Diphenyl-1,4-dihydro-1,2,4-benzotriazin-4-yls: An Improved Synthesis of Blatter's Radical. *Synthesis* **2010**, *2010*, 2075-2079.

19. Berezin, A. A.; Constantinides, C. P.; Mirallai, S. I.; Manoli, M.; Cao, L. L.; Rawson, J. M.; Koutentis, P. A. Synthesis and properties of imidazolo-fused benzotriazinyl radicals. *Org. Biomol. Chem.* **2013**, *11*, 6780-6795.

20. Berezin, A. A.; Zissimou, G.; Constantinides, C. P.; Beldjoudi, Y.; Rawson, J. M.; Koutentis, P. A. Route to Benzo- and Pyrido-Fused 1,2,4-Triazinyl Radicals via *N*′-(Het)aryl-*N*′-[2-nitro(het)aryl]hydrazides. *J. Org. Chem.* **2014**, *79*, 314-327.

21. Savva, A. C.; Mirallai, S. I.; Zissimou, G. A.; Berezin, A. A.; Demetriades, M.; Kourtellaris, A.; Constantinides, C. P.; Nicolaides, C.; Trypiniotis, T.; Koutentis, P. A. Preparation of

Blatter Radicals via Aza-Wittig Chemistry: The Reaction of *N*-Aryliminophosphoranes with 1-(Het)aroyl-2-aryldiazenes. *J. Org. Chem.* **2017**, *82*, 7564-7575.

22. Berezin, A. A.; Constantinides, C. P.; Drouza, C.; Manoli, M.; Koutentis, P. A. From Blatter Radical to 7-Substituted 1,3-Diphenyl-1,4-dihydrothiazolo[5′,4′:4,5]benzo[1,2-*e*][1,2,4]triazin-4-yls: Toward Multifunctional Materials. *Org. Lett.* **2012**, *14*, 5586-5589.

23. Constantinides, C. P.; Koutentis, P. A.; Loizou, G. Synthesis of 7-aryl/heteraryl-1,3-diphenyl-1,2,4-benzotriazinyls via palladium catalyzed Stille and Suzuki-Miyaura reactions. *Org. Biomol. Chem.* **2011**, *9*, 3122-3125.

24. Constantinides, C. P.; Obijalska, E.; Kaszynski, P. Access to 1,4-Dihydrobenzo[*e*]-[1,2,4]triazin-4-yl Derivatives. *Org. Lett.* **2016**, *18*, 916-919.

25. Grant, J. A.; Lu, Z.; Tucker, D. E.; Hockin, B. M.; Yufit, D. S.; Fox, M. A.; Kataky, R.; Chechik, V.; O'Donoghue, A. M. C. New Blatter-type radicals from a bench-stable carbene. *Nat. Commun.* **2017**, *8*, 15088.

26. Kaszynski, P.; Constantinides, C. P.; Young, V. G The Planar Blatter Radical: Structural Chemistry of 1,4-Dihydrobenzo[*e*][1,2,4]triazin-4-yls. *Angew. Chem. Int. Ed.* **2016**, *55*, 11149-11152.

27. Takahashi, Y.; Miura, Y.; Yoshioka, N. Introduction of Three Aryl Groups to Benzotriazinyl Radical by Suzuki–Miyaura Cross-coupling Reaction. *Chem. Lett.* **2014**, *43*, 1236-1238.

28. Constantinides, C. P.; Koutentis, P. A.; Rawson, J. M. Antiferromagnetic Interactions in 1D Heisenberg Linear Chains of 7-(4-Fluorophenyl) and 7-Phenyl-Substituted 1,3-Diphenyl-1,4-dihydro-1,2,4-benzotriazin-4-yl Radicals. *Chem. - Eur. J.* **2012**, *18*, 15433-15438.

29. Constantinides, C. P.; Berezin, A. A.; Manoli, M.; Leitus, G. M.; Zissimou, G. A.; Bendikov, M.; Rawson, J. M.; Koutentis, P. A. Structural, Magnetic, and Computational Correlations of Some Imidazolo-Fused 1,2,4-Benzotriazinyl Radicals. *Chem. - Eur. J.* **2014**, *20*, 5388-5396.

30. Constantinides, C. P.; Koutentis, P. A.; Rawson, J. M. Ferromagnetic Interactions in a 1D Alternating Linear Chain of π-Stacked 1,3-Diphenyl-7-(thien-2-yl)-1,4-dihydro-1,2,4-benzotriazin-4-yl Radicals. *Chem. - Eur. J.* **2012**, *18*, 7109-7116.

31. Constantinides, C. P.; Berezin, A. A.; Manoli, M.; Leitus, G. M.; Bendikov, M.; Rawson, J. M.; Koutentis, P. A. Effective exchange coupling in alternating-chains of a π-extended 1,2,4-benzotriazin-4-yl. *New J. Chem.* **2014**, *38*, 949-954.

32. Constantinides, C. P.; Berezin, A. A.; Zissimou, G. A.; Manoli, M.; Leitus, G. M.; Bendikov, M.; Probert, M. R.; Rawson, J. M.; Koutentis, P. A. A Magnetostructural Investigation of an Abrupt Spin Transition for 1-Phenyl-3-trifluoromethyl-1,4-dihydrobenzo[*e*][1,2,4]triazin-4-yl. *J. Am. Chem. Soc.* **2014**, *136*, 11906-11909.

33. Constantinides, C. P.; Carter, E.; Murphy, D. M.; Manoli, M.; Leitus, G. M.; Bendikov, M.; Rawson, J. M.; Koutentis, P. A. Spin-triplet excitons in 1,3-diphenyl-7-(fur-2-yl)-1,4-dihydro-1,2,4-benzotriazin-4-yl. *Chem. Commun.* **2013**, *49*, 8662-8664.

34. Constantinides, C. P.; Berezin, A. A.; Zissimou, G. A.; Manoli, M.; Leitus, G. M.; Koutentis, P. A. The Suppression of Columnar π-Stacking in 3-Adamantyl-1-phenyl-1,4-dihydrobenzo[*e*][1,2,4]triazin-4-yl. *Molecules* **2016**, *21*, 636.

35. Takahashi, Y.; Matsuhashi, R.; Miura, Y.; Yoshioka, N. Magnetic Interactions through a Nonconjugated Framework Observed in Back-to-Back Connected Triazinyl–Nitroxyl Biradical Derivatives. *Chem. - Eur. J.* **2018**, *24*, 7939-7948.

36. Takahashi, Y.; Tsuchiya, N.; Miura, Y.; Yoshioka, N. Magneto-structural correlation of cyano-substituted 3-*tert*-butyl-1-phenyl-1,2,4-benzotriazin-4-yl: spin transition behaviour observed in a 6-cyano derivative. *New. J. Chem.* **2018**, *42*, 9949-9955.

37. Zheng, Y.; Miao, M.-s.; Kemei, M. C.; Seshadri, R.; Wudl, F. The Pyreno-Triazinyl Radical – Magnetic and Sensor Properties. *Isr. J. Chem.* **2014**, *54*, 774-778.

38. Miura, Y.; Yoshioka, N. π-Stacked structure of thiadiazolo-fused benzotriazinyl radical: Crystal structure and magnetic properties. *Chem. Phys. Lett.* **2015**, *626*, 11-14.

39. Hu, X.; Zhao, L.; Chen., H.; Ding, Y.; Zheng, Y.-Z.; Miao, M.-s.; Zheng, Y. Air stable high-spin blatter diradicals: non-Kekulé versus Kekulé structures. *J. Mater. Chem. C* **2019**, *7*, 6559-6563.

40. Yan, B.; Cramer, J.; McDonald, R.; Frank, N. L. Ferromagnetic spin-delocalized electron donors for multifunctional materials: π-conjugated benzotriazinyl radicals. *Chem. Commun.* **2011**, *47*, 3201-3203.

41. Takahashi, Y.; Miura, Y.; Yoshioka, M. Synthesis and properties of the 3-*tert*-butyl-7-trifluoromethyl-1,4-dihydro-1-phenyl-1,2,4-benzotriazin-4-yl radical. *New J. Chem.* **2015**, *39*, 4783-4789.

42. Demetriou, M.; Berezin, A. A.; Koutentis, P. A.; Krasia-Christoforou, T.; Benzotriazinyl-mediated controlled radical polymerization of styrene. *Polym. Int.* **2014**, *63*, 674-679.

43. Areephong, J.; Mattson, K. M.; Treat, N. J.; Poelma, S. O.; Kramer, J. W.; Sprafke, H. A.; Latimer, A. A.; Read de Alaniz, J.; Hawker, C. J. Triazine-mediated controlled radical polymerization: new unimolecular initiators. *Polym. Chem.* **2016**, *7*, 370-374.

44. Areephong, J.; Treat, N.; Kramer, J. W.; Christianson, M. D.; Hawker, C. J.; Collins, H. A. *WO Pat.*, 061189A1, **2015**.

45. Rogers, F. J. M.; Coote, M. L. Computational Evaluation of the Oxidative Cleavage of Triazine Derivatives for Electrosynthesis. *J. Phys. Chem. C* **2019**, *123*, 10306-10310.

46. Morgan, I. S.; Peuronen, A.; Hänninen, M. M.; Reed, R. W.; Clérac, R.; Tuononen, H. M. 1-Phenyl-3-(pyrid-2-yl)benzo[*e*][1,2,4]triazinyl: The First "Blatter Radical" for Coordination Chemistry. *Inorg. Chem.* **2014**, *53*, 33-35.

47. Morgan, I. S.; Mansikkamäki, A.; Loizou, G. A.; Koutentis, P. A.; Rouzières, M.; Clérac, R.; Tuononen, H. M. Coordination Complexes of a Neutral 1,2,4-Benzotriazinyl Radical Ligand: Synthesis, Molecular and Electronic Structures, and Magnetic Properties. *Chem. - Eur. J.* **2015**, *21*, 15843-15853.

48. Morgan, I. S.; Mansikkamäki, A.; Rouzières, M.; Clérac, R.; Tuononen, H. M. Coexistence of long-range antiferromagnetic order and slow relaxation of the magnetization in the first lanthanide complex of a 1,2,4-benzotriazinyl radical. *Dalton Trans.* **2017**, *46*, 12790-12793.

49. Poryvaev, A. S.; Polyukhov, D. M.; Gjuzi, E.; Hoffmann, F.; Fröba, M.; Fedin, M. V. Radical-Doped Metal–Organic Framework: Route to Nanoscale Defects and Magnetostructural Functionalities. *Inorg. Chem.* **2019**, *58*, 8471-9479.

50. Gallagher, N.; Zhang, H.; Junghoefer, T.; Giangrisostomi, E.; Ovsyannikov, R.; Pink, M.; Rajca, S.; Casu, M. B.; Rajca, A. Thermally and Magnetically Robust Triplet Ground State Diradical. *J. Am. Chem. Soc.* **2019**, *141*, 4764-4774.

51. Karecla, G.; Papagiorgis, P.; Panagi, N.; Zissimou, G. A.; Constantinides, C. P.; Koutentis, P. A.; Itskos, G.; Hayes, S. C. Emission from the stable Blatter radical. *New J. Chem.* **2017**, *41*, 8604-8613.

52. Zhang, Y.; Zheng, Y.; Zhou, H.; Miao, M.-S.; Wudl, F.; Nguyen, T.-Q. Temperature Tunable Self-Doping in Stable Diradicaloid Thin-Film Devices. *Adv. Mater.* **2015**, *27*, 7412-7419.

53. Zheng, Y.; Miao, M.-S.; Dantelle, G.; Eisenmenger, N. D.; Wu, G.; Yavuz, I.; Chabinyc, M. L.; Houk, K. N.; Wudl, F. A Solid-State Effect Responsible for an Organic Quintet State at Room Temperature and Ambient Pressure. *Adv. Mater.* **2015**, *27*, 1718-1723.

54. Jasinski, M.; Kapuscinski, S.; Kaszynski, P. Stability of a columnar liquid crystalline phase in isomeric derivatives of the 1,4-dihydrobenzo[*e*][1,2,4]triazin-4-yl: Conformational effects in the core. *J. Mol. Liq.* **2019**, *277*, 1054-1059.

55. Jasinski, M.; Szymanska, K.; Gardias, A.; Pociecha, D.; Monobe, H.; Szczytko, J.; Kaszynski, P. Tuning the Magnetic Properties of Columnar Benzo[*e*][1,2,4]triazin-4-yls with the Molecular Shape. *ChemPhysChem* **2019**, *20*, 636-644.

56. Kapuscinski, S.; Gardias, A.; Pochiecha, D.; Jasinski, M.; Szczytko, J.; Kaszynksi, P. Magnetic behaviour of bent-core mesogens derived from the 1,4-dihydrobenzo[*e*]-[1,2,4]triazin-4-yl. *J. Mater. Chem. C* **2018**, *6*, 3079-3088.

57. Jasinski, M.; Szczytko, J.; Pochiecha, D.; Monobe, H.; Kaszynski, P. Substituent-Dependent Magnetic Behavior of Discotic Benzo[*e*][1,2,4]triazinyls. *J. Am. Chem. Soc.* **2016**, *138*, 9421-9424.

58. Häupler, B.; Schubert, U. S.; Wild, A.; Koutentis, P. A.; Zissimou, G. *DE Pat.,* 102017005 924A1, **2018**.

59. Saal, A.; Friebe, C.; Schubert, U. S. Blatter radical as a polymeric active material in organic batteries. *J. Power Sources* **2022**, 231061(1-10).

60. Steen, J. S.; Nuismer, J. L.; Eiva, V.; Wiglema, A. E. T.; Daub, N.; Hjelm, J.; Otten, E. Blatter radicals as Bipolar Materials for Symmetrical Redox-Flow Batteries. *J. Am. Chem. Soc.* **2022**, *144*, 5051-5058.

61. Ciccullo, F.; Gallagher, N. M.; Geladari, O.; Chassé, T.; Rajca, A.; Casu, M. B. A Derivative of the Blatter Radical as a Potential Metal-Free Magnet for Stable Thin Films and Interfaces. *ACS Appl. Mater. Interfaces* **2016**, *8*, 1805-1812.

62. Casu, M. B. Nanoscale Studies of Organic Radicals: Surface, Interface, and Spinterface. *Acc. Chem. Res.* **2018**, *51*, 753-760.

63. Low, J. Z.; Kladnik, G.; Patera, L. L.; Sokolov, S.; Lovat, G.; Kumarasamy, E.; Repp, J.; Campos, L. M.; Cvetko, D.; Morgante, A.; Venkataraman, L. The Environment-Dependent Behavior of the Blatter Radical at the Metal–Molecule Interface. *Nano Lett.* **2019**, *19*, 2543-2548.

64. Patera, L. L.; Sokolov, S.; Low, J.; Campos, L.; Venkataraman, L.; Repp, J. Resolving the Unpaired-Electron Orbital Distribution in a Stable Organic Radical by Kondo Resonance Mapping. *Angew. Chem. Int. Ed.* **2019**, *58*, 11063-11067.

65. Ciccullo, F.; Calzolari, A.; Bader, K.; Neugebauer, P.; Gallagher, N. M.; Rajca, A.; van Slageren, J.; Casu, M. B. Interfacing a Potential Purely Organic Molecular Quantum Bit with a Real-Life Surface. *ACS Appl. Mater. Interfaces* **2019**, *11*, 1571-1578.

66. Nicolaides, C.; Bazzi, F.; Vouros, E.; Flesariu, D. F.; Chrysochos, N.; Koutentis, P. A.; Constantinides, C. P.; Trypiniotis, T. Metal-Free Organic Radical Source *Nano Lett.* **2023**, *23*, 4579-4586.

67. Perras, F. A.; Flesariu, D. F.; Southern, S. A.; Nicolaides, C.; Bazak, J. D.; Washton, N. M.; Trypiniotis, T.; Constantinides, C. P.; Koutentis, P. A. Methyl-Driven Overhauser Dynamic Nuclear Polarization. *J. Phys. Chem. Lett.* **2022**, *13*, 4000-4006.

68. Perras, F. A.; Matsuki, Y.; Southern, S. A.; Dubroca, T.; Flesariu, D. G.; Van Tol, J.; Constantinides, C. P.; Koutentis, P. A. Mechanistic origins of methyl-driven Overhauser DNP. *J. Chem. Phys.* **2023**, *158*, 154201.

69. Boudalis, A. K.; Constantinides, C. P.; Chrysochos, N.; Carmieli, R.; Leitus, G.; Kourtellaris, A.; Lawson, D. B.; Koutentis, P. A. Deciphering the ground state of a C_3-symmetrical Blatter-type triradical by CW and pulse EPR spectroscopy. *J. Magn. Reson.* **2023**, *349*, 107406(1-9).

70. Constantinides, C. P.; Lawson, D. B.; Berezin, A. A.; Zissimou, G. A.; Manoli, M.; Leitus, G. M.; Koutentis, P. A. Ferromagnetic interactions in a 1D Heisenberg linear chain of 1-

phenyl-3,7-bis(trifluoromethyl)-1,4-dihydro-1,2,4-benzotriazin-4-yls. *CrystEngComm* **2019**, *21*, 4599-4606.

71. Bazzi, F.; Danke, A. J.; Lawson, D. B.; Manoli, M.; Leitus, G. M.; Koutentis, P. A.; Constantinides, C. P. 1-(2-Methoxyphenyl)-3-phenyl-1,4-dihydro-1,2,4-benzotriazin-4-yl: a tricky "structure-to-magnetism" correlation aided by DFT calculations. *CrystEngComm* **2020**, *22*, 4306-4316.

72. Constantinides, C. P.; Lawson, D. B.; Zissimou, G. A.; Berezin, A. A.; Mailman, A.; Manoli, M.; Kourtellaris, A.; Leitus, G. M.; Clérac, R.; Tuononen, H. M.; Koutentis, P. A. Polymorphism in a π-stacked Blatter radical: structures and magnetic properties of 3-(phenyl)-1-(pyrid-2-yl)-1,4-dihydrobenzo[*e*][1,2,4]triazin-4-yl. *CrystEngComm* **2020**, *22*, 5453-5463.

73. Novoa, J. J.; Deumal, M.; Jornet-Somoza, J. Calculation of microscopic exchange interactions and modelling of macroscopic magnetic properties in molecule-based magnets. *Chem. Soc. Rev.* **2011**, *40*, 3182-3212.

74. Blanchard, S.; Neese, F.; Bothe, E.; Bill, E.; Weyhermüller, T.; Wieghardt, K. Square Planar vs Tetrahedral Coordination in Diamagnetic Complexes of Nickel(II) Containing Two Bidentate π-Radical Monoanions. *Inorg. Chem.* **2005**, *44*, 3636-3656.

75. Fauconnier, T.; Lock, C. J. L.; Bell, R. A.; Britten, J. F.; Rainsford, K. D. Studies of nonsteroidal anti-inflammatory drugs: azapropazone. *Can. J. Chem.* **1994**, *72*, 382-389.

76. Al-Noaimi, M. Z.; Abdel-Jalil, R. J.; El-Abadelah, M. M.; Haddad, S. F.; Baqi, Y. N. H.; Voelter, W. Metal-Assisted Oxidative Cyclization of Arylamidrazones I. Synthesis of 3-Acetyl-1,4-dihydro-1-phenyl-1,2,4-benzotriazine. *Monatsh. Chem.* **2006**, *137*, 745-750.

77. Gardias, A.; Kaszynski, P.; Obijalska, E.; Trzybinski, D.; Domagala, S.; Wozniak, K.; Szczytko, J. Magnetostructural Investigation of Orthogonal 1-Aryl-3-Phenyl-1,4-Dihydrobenzo[*e*][1,2,4]triazin-4-yl Derivatives. *Chem. - Eur. J.* **2018**, *24*, 1317-1329.

78. Bray, J. W.; Interrante, L.V.; Jacobs, I. S.; Bonner, J. C. *The Spin-Peierls Transition*, *In Extended Linear Chain Compound.*, J. S. Miller (Ed.), Springer, Boston, MA, **1983**.

79. Pouget, J.-P.; Alemany, P.; Canadell, E. Donor–anion interactions in quarter-filled low-dimensional organic conductors. *Mater. Horiz.* **2018**, *5*, 590-640.

80. Clay, R. T.; Mazumdar, S. From charge- and spin-ordering to superconductivity in the organic charge-transfer solids. *Phys. Rep* **2019**, *788*, 1-89.

81. Vasiliev, A.; Volkova, O.; Zvereva, E.; Markina, M. Milestones of low-D quantum magnetism. *npj Quantum Mater.* **2018**, *3*, 18.

82. Duan, H.-B.; Ren, X.-M.; Meng, Q.-J. One-dimensional (1D) [Ni(mnt)2]¯-based spin-Peierls-like complexes: Structural, magnetic and transition properties. *Coord. Chem. Rev.* **2010**, *254*, 1509-1522.

83. Coulon, C.; Clérac, R. Electron Spin Resonance: A Major Probe for Molecular Conductors. *Chem. Rev.* **2004**, *104*, 5655-5687.

84. Bonner, J. C.; Fisher, M. E. Linear Magnetic Chains with Anisotropic Coupling. *Phys. Rev.* **1964**, *135*, A640-A658.

85. Torrance, J. B.; Tomkiewicz, Y.; Silverman, B. D. Enhancement of the magnetic susceptibility of TTF-TCNQ (tetrathiafulvalene-tetracyanoquinodimethane) by Coulomb correlations. *Phys. Rev. B* **1977**, *15*, 4738-4749.

86. Estes, W. E.; Gavel, D. P.; Hatfield, W. E.; Hodgson, D. J. Magnetic and structural characterization of dibromo- and dichlorobis(thiazole)copper(II). *Inorg. Chem.* **1978**, *17*, 1415-1421.

87. Clarke, C. S.; Jornet-Somoza, J.; Mota, F.; Novoa, J. J.; Deumal, M. Origin of the Magnetic Bistability in Molecule-Based Magnets: A First-Principles Bottom-Up Study of the TTTA Crystal. *J. Am. Chem. Soc.* **2010**, *132*, 17817-17830.

88. Vela, S.; Mota, F.; Deumal, M.; Suizu, R.: Shuku, Y.; Mizuno, A.; Awaga, K.; Shiga, M.; Novoa, J. J.; Ribas-Arino, J. The key role of vibrational entropy in the phase transitions of dithiazolyl-based bistable magnetic materials. *Nat. Commun*. **2014**, *5*, 4411.

89. Vela, S.; Deumal, M.; Shiga, M.; Novoa, J. J.; Ribas-Arino, J. Dynamical effects on the magnetic properties of dithiazolyl bistable materials. *Chem. Sci.* **2015**, *6*, 2371-2381.

90. Kahn, O.; Morgenstern-Badarau, I.; Audiere, J. P.; Lehn, J. M.; Sullivan, S. A. Exchange elasticity in copper(II) dinuclear cryptates. *J. Am. Chem. Soc.* **1980**, *102*, 5935-5936.

91. Constantinides, C. P.; Eisler, D. J.; Alberola, A.; Carter, E.; Murphy, D. M.; Rawson, J. M. Weakening of the π^*–π^* dimerisation in 1,2,3,5-dithiadiazolyl radicals: structural, EPR,

magnetic and computational studies of dichlorophenyl dithiadiazolyls, $Cl_2C_6H_3CNSSN$. *CrystEngComm* **2014**, *16*, 7298-7312.

92. Constantinides, C. P.; Carter, E.; Eisler, D.; Beldjoudi, Y.; Murphy, D. M.; Rawson, J. M. Effects of Halo-Substitution on 2′-Chloro-5′-halo-phenyl-1,2,3,5-dithiadiazolyl Radicals: A Crystallographic, Magnetic, and Electron Paramagnetic Resonance Case Study. *Cryst. Growth Des.* **2017**, *17*, 3017-3029.

93. Takahashi, K.; Shirakawa, Y.; Sakai, H.; Hisaki, I.; Noro, S.-i.; Akutagawa, T.; Nakano, M.; Nakamura, T. Uniaxial negative thermal expansion induced by molecular rotation in a one-dimensional supramolecular assembly with associated peculiar magnetic behavior. *J. Mater. Chem. C* **2023**, *11*, 1891-1898.

94. Sheppard, C. L.; Tandon, S. S.; Thompson, L. K.; Bridson, J. N.; Miller, D. O.; Handa, M.; Lloret, F. Polynuclear copper(II) complexes with μ_2-1,1-azide bridges. Structural and magnetic properties. *Inorg. Chim. Acta* **1996**, *250*, 227-239.

95. Muthukumaran, R.; Chandramouli, G. V. R.; Manoharan, P. T. Intra and intermodular exchange interactions in bis(α-aminoisobutyrato)oxalamidodicopper(Aib-COCO-Aib)Cu_2. *Chem. Phys. Lett.* **2005**, *404*, 227-231.

96. Deumal, M.; Bearpark, M. J.; Novoa, J. J.; Robb, M. A. Magnetic properties of organic molecular crystals via an Algebraic Heisenberg Hamiltonian. Applications to WILVIW, TOLKEK, and KAXHAS Nitronyl Nitroxide Crystals. *J. Phys. Chem. A* **2002**, *106*, 1299-1315.

97. Fumanal, M.; Jornet-Somoza, J.; Vela, S.; Novoa, J. J.; Ribas-Arino, J.; Deumal, M. Pitfalls on evaluating pair exchange interactions for modelling molecule-based magnetism. *J. Mater. Chem. C* **2021**, *9*, 10647-10660.